Direct Access to Optical Aberration Information in Fluorescence Laser Scanning Microscopy Using Detector Arrays

Francesco Fersini[a,b], Alessandro Zunino[a], Pietro Morerio[c], Alessio Del Bue[c], Martin J. Booth[d], and Giuseppe Vicidomini[a]

[a]Molecular Microscopy and Spectroscopy, Istituto Italiano di Tecnologia, Genoa, Italy,
[b]DIBRIS, University of Genoa, Genoa, Italy
[c]Pattern Analysis and Computer Vision, Pavis, Genoa, Italy
[d]Department of Engineering Science, University of Oxford, Oxford, UK

ABSTRACT

In the recent years, numerous adaptive optics techniques have emerged to address optical aberrations in fluorescence microscopy imaging. However, many existing methods involve complex hardware implementations or lengthy iterative algorithms that may induce photo-damage to the sample. Our study proposes an innovative approach centered around a novel detector array capable of potentially capturing the probed sample in a single acquisition. Our solution is gentle on the sample and applicable to any laser scanning microscope equipped with a detector array. We demonstrate that the multi-dimensional dataset obtained using the detector array inherently encodes information about optical aberrations. Finally, we propose a convolutional neural network approach to decode these optical aberrations in real-time and with high accuracy, establishing the foundation for a new class of adaptive optics laser-scanning microscopy methods.

Keywords: Adaptive optics, Image scanning microscope, detector array, deep learning, convolutional neural network, optical aberration, deep imaging, fluorescence

1. INTRODUCTION

Image Scanning Microscopy (ISM) has emerged as a natural advancement in confocal microscopy, elevating it to a practical super-resolution technique.[1–4] In the ISM architecture based on laser-scanning microscopy, this transformation entails the replacement of the standard singular-point detector and pinhole in the detection arm with a detector array. This modification upgrades conventional Confocal Laser Scanning Microscopes (CLSM) into ISM configurations. Presently, the most powerful detector array for implementing ISM in laser-scanning microscopy is represented by asynchronous read-out single-photon-avalanche diode (SPAD) array detectors.[5,6] The single-photon timing capability of these detectors has also facilitated their integration with time-resolved spectroscopy, resulting in further advancements in ISM and laser-scanning microscopy in general. In particular, these detector arrays have proven advantageous in enhancing resolution and contrast for imaging,[7–10] and improving information content and flexibility in fluorescence correlation spectroscopy.[11] Significantly, despite the physical pinhole being removed, the advantages of ISM described above can be achieved without compromising the optical sectioning ability typical of confocal microscopy[12] – an essential feature when conducting imaging in deep samples .

Further author information: giuseppe.vicidomini@iit.it

Adaptive Optics and Wavefront Control for Biological Systems X, edited by
Thomas G. Bifano, Na Ji, Lei Tian, Proc. of SPIE Vol. 12851, 1285102
 · 1605-7422 · doi: 10.1117/12.3000914

Confocal laser-scanning microscopy seeks to achieve super-resolution by reducing the size of the point-spread function (PSF) through optical pinhole closure.[13–15] However, this strategy induces substantial signal loss, resulting in a diminished signal-to-noise ratio (SNR). In contrast, ISM leverages the detector array elements as small virtual pinholes, enabling simultaneous and independent confocal image collection without discarding any fluorescent photons. More specifically, the data acquisition process in ISM yields a multi-dimensional dataset, comprising a sequence of 2D confocal scanned images corresponding to the detector array elements or, equivalently, a series of micro-images of as many as the scanning points (i.e., pixel of the conventional scanning image).

This study demonstrates how this innovative ISM dataset facilitates comprehensive insights into the PSF of the optical system and concurrently reveals information about optical aberrations. Notably, whether the optical aberration originating from the system or specimen, can substantially compromise resolution and optical sectioning, even within the ISM framework.

Adaptive optics systems emerge as versatile solutions, allowing tailored optical adjustments of the wavefront of light to generate aberration-free PSFs, achieved through the integration of dynamic adaptive elements such as a deformable mirror (DM) or spatial light modulator (SLM). However, the current limitation of adaptive optics lies in its capacity to identify optical aberrations with straightforward instrumentation and a non-invasive approach for the sample.[16–20] In recent years, numerous wavefront sensing and control strategies have been devised to address optical aberrations. However, these often involve complex imaging systems or iterative algorithms that may compromise sample integrity. This paper introduces a novel, simple, and gentle approach for optical aberration encoding in any image-scanning microscope. The proposed methodology aims to present an alternative to existing wavefront sensors or phase retrieval algorithms by employing a detector array for imaging and as an intrinsic wavefront sensor.

2. RESULTS AND DISCUSSION

In any confocal laser scanning microscopy setup, the focused excitation laser beam systematically illuminates the sample through point-by-point raster scanning across the sample-plane coordinates $\mathbf{x_s} = (x_\mathrm{s}, y_\mathrm{s})$ (Fig. 1 a). The fluorescent light emitted by the sample is filtered by the pinhole to reject the out-of-focus component, and the intensity value accumulated during the pixel's dwell time is captured by the single-photon detector, typically a photo-multiplier tube, enabling the progressive formation of the image. In image scanning microscopy, while the illumination follows the same principles of CLSM, the image formation process deviates by employing a detector array, whose elements – 5×5 elements as for our SPAD array detector – act as a series of virtual and parallel pinholes (Fig. 1 b). Thereby, not a single images, but a series of scanned confocal images, one images for each element of the detector array, are formed progressively.[10] The PSF associated to the scanned image generated by an element of the detector array at the position $\mathbf{x_d} = (x_\mathrm{d}, y_\mathrm{d})$ reads:

$$\begin{aligned} h(\mathbf{x_s} \mid \mathbf{x_d}) &= h_{exc}(-\mathbf{x_s}) \cdot [h_{emi}(\mathbf{x_s}) * \mathrm{p}(\mathbf{x_s} - \mathbf{x_d})] \\ &= h_{exc}(-\mathbf{x_s}) \cdot h_{det}(\mathbf{x_s} - \mathbf{x_d}) \end{aligned} \tag{1}$$

where, p denotes the pinhole aperture, represented by the active area of each detector element. The functions h_{exc} and h_{emi} correspond to the excitation and emission PSFs of the microscope, respectively. The detection PSF h_{det} is defined as the convolution product of h_{emi} with the pinhole p.

Consequently, the image formation for the scanned image associated with the element at position $\mathbf{x_d}$ reads:

$$i(\mathbf{x}_\mathrm{s} \mid \mathbf{x}_\mathrm{d}) = o(\mathbf{x}_\mathrm{s}) * h(\mathbf{x}_\mathrm{s} \mid \mathbf{x}_\mathrm{d}). \tag{2}$$

The PSFs associated with each detector element are derived from the multiplication of two peak functions – the excitation and detection functions. The excitation functions are identical for each detector element, while the emission functions are nearly identical, with a shift determined by the geometry of the detector array. This results in approximately identical PSFs, with the only difference being a shift. Consequently, due to the near-identical PSFs except for the shift, the scanned images $i(\mathbf{x}\mathrm{s} \mid \mathbf{x}\mathrm{d})$ are, in a first approximation, nearly identical except for a shift and an intensity rescaling (Fig. 1 c).

The shift of each scanned image – concerning the central one – is termed the *shift-vector*, and it generally depends not only on the geometry of the detector array, but also on both the excitation and detection PSFs parameters. To estimate these shift-vectors $\boldsymbol{\mu}(\mathbf{x}\mathrm{d})$, one can apply a phase correlation algorithm, commonly used for estimating drift between two images of the same object. Notably, the phase correlation-based estimation of shift-vectors forms the foundation of adaptive pixel-reassignment (APR) method.[7,10,21] This method is employed to reconstruct a high-resolution and high-SNR image from the raw scanned images. Once the shift-vectors are estimated, each scanned image is shifted by the respective amount, and all are then summed together. In other words, the pixel reassignment method registers the scanned images and subsequently integrates their signals.

Alongside the shift-vectors, another figure of merit capable of characterizing the scanned image, and more broadly, the ISM imaging system, is the so-called *fingerprint* (Fig. 1 d). This is obtained by integrating the PSF in Eq. 1 over the scanning coordinates $\mathbf{x_s}$:

$$\begin{aligned} f(\mathbf{x}_\mathrm{d}) = \int_{\mathbb{R}^2} h(\mathbf{x}_\mathrm{s} \mid \mathbf{x}_\mathrm{d})\, d\mathbf{x}_\mathrm{s} &= \int_{\mathbb{R}^2} h_\mathrm{exc}(-\mathbf{x}_\mathrm{s}) \cdot h_\mathrm{emi}(\mathbf{x}_\mathrm{s} - \mathbf{x}_\mathrm{d})\, d\mathbf{x}_\mathrm{s} \\ &= (h_\mathrm{exc} * h_\mathrm{emi})(\mathbf{x}_\mathrm{d}). \end{aligned} \tag{3}$$

It can be readily shown that, apart from a scaling factor, the fingerprint can also be derived by integrating the scanned images over the scanning coordinates $\mathbf{x_s}$.[7,12] This implies that the fingerprint distribution possesses important properties, being independent of the observed sample and merely a characteristic of the imaging system.

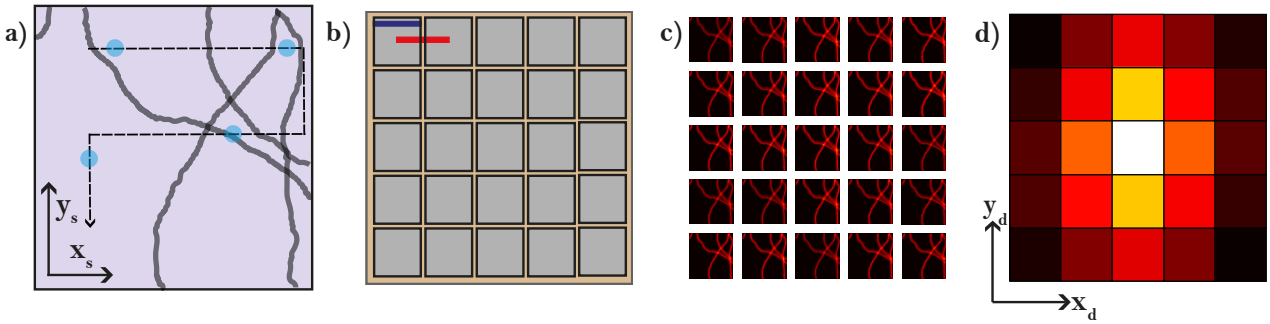

Figure 1. a) Illustration of the point-by-point scanning process in a laser scanning microscope across the sample plane. The dashed line corresponds to the path of the excitation beam, highlighted with the blue circle. b) The ISM dataset comprises images equal to the number of elements in the detector array, where each element acts as a single pinhole. The sensor dimensions are shown in blue (50 µm), and the distance pitch in red (75 µm). c) The ISM dataset, viewed as a fingerprint with respect to the element coordinates $(\mathbf{x}_\mathrm{d})$ d) The ISM dataset, viewed as a collection of scanned images with respect to the scanning coordinates $(\mathbf{x}_\mathrm{s})$, for elements of the detector array.

While it is visible to reconstruct a high-resolution image via pixel reassignment under the assumption that the PSFs of the scanned images are identical except for a shift, this approximation overlooks important properties of the optical system.

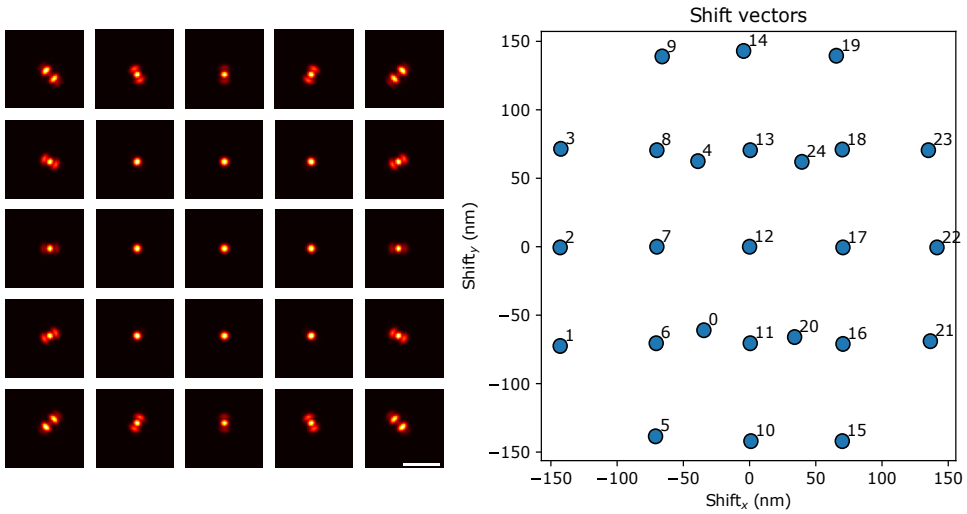

Figure 2. Simulated scanned images of a gold bead 80 nm, arranged as the corresponding detector element, and distribution of the shift-vector of the whole ISM dataset, obtained with the APR algorithm. Scale bar 500 nm. The peripheral images show multiple maxima due to the presence of diffraction rings. Scale bar 1 µm.

Due to the presence of diffraction rings in the illumination and detection PSF and possible optical aberrations, the PSFs of the different scanned image, in general, differ not only in position but also in shape. The most distorted PSFs are associated with the most peripheral elements of the detector array, where the effect of diffraction rings dominates (see Fig. 2).

In the presence of optical aberrations, the multi-dimensional dataset, comprising both the fingerprint and shift-vectors, becomes highly sensitive to these aberrations. Optical aberrations introduce modifications in the phase propagation of both the h_{exc} and h_{det} PSFs, consequently impacting the distribution of light within the detector plane. Consequently, the fingerprint serves as a valuable indicator for optical aberrations, providing insights into information that would otherwise be overlooked when using typical single-element detectors, as in CLSM.

It is crucial to note that, although compensating for optical aberrations ultimately requires adaptive optics elements to correct the distortion of the wavefront for both excitation and emission, a partial compensation of optical aberrations is achieved through the adaptive pixel reassignment method. This technique serves as an initial step in mitigating optical aberration effects. The adaptive pixel reassignment method functions by estimating the maximum correlation between images, enabling the correct summation of images by applying the appropriate shifts, even in the presence of pronounced optical aberrations.

However, the more intriguing aspect is studying how imaging with the detector array can effectively encode information about optical aberrations—both induced by the sample and/or the optical elements of the microscope architecture. To investigate this capability, we conducted a set of simulated experiments using the open-source simulator tool known as BrightEyes-ISM.[22] Developed as a computational toolbox, this simulator serves the scientific community by offering advanced algorithms for processing ISM datasets (e.g., image reconstruction and image quality evaluation) and simulating the image formation process. Implemented as a Python package, BrightEyes-ISM comprises three distinct modules, each tailored for specific requests: data loading, data analysis, and image simulations. The simulation module comprises two key components: a PSF calculation module and a synthetic sample generation module, mimicking a network of tubulin filaments (Fig. 3 a-b). Integrating PyFocus – a Python package enabling vectorial calculations of focused optical fields – into BrigthEyes-ISM the PSF simulator can generate the series of PSFs for ISM, including also the possibility to simulate different optical aberrations.

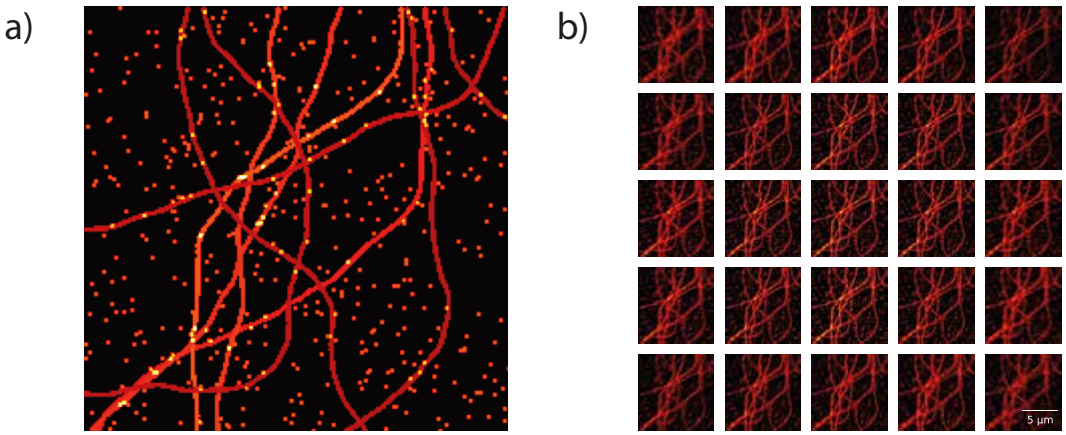

Figure 3. a) Simulation of tubulin filament and beads. Pixel size, diameter of the phantoms number, and thickness can be tuned. b) Image a) convoluted with a set of simulated PSFs λ_{ex} = 488 nm, λ_{em} = 515 nm, M = 550, NA = 1.4, phase mask sampling = 200.

Image scanning microscopy can be characterised by a series of PSFs, each PSF corresponds to an element of the detector array, incorporating all relevant physical parameters that can be finely adjusted, including the possibilty to integrate different phase mask for the incoming wave of light. These phase masks can be used to simulate the PSFs with different optical abberations. Subsequently, these PSFs undergo convolution with a realistic phantom, introducing both Poissonian noise related to the photon counting nature of the experiment and dark noise related to the characteristics of the SPAD detector elements

Using BrightEyes-ISM we started to explore the impact of aberrations on the ISM multi-dimensional dataset. We developed a phase mask calculator enabling the introduction of any aberration or a user-defined phase mask as shown in Fig. 4.

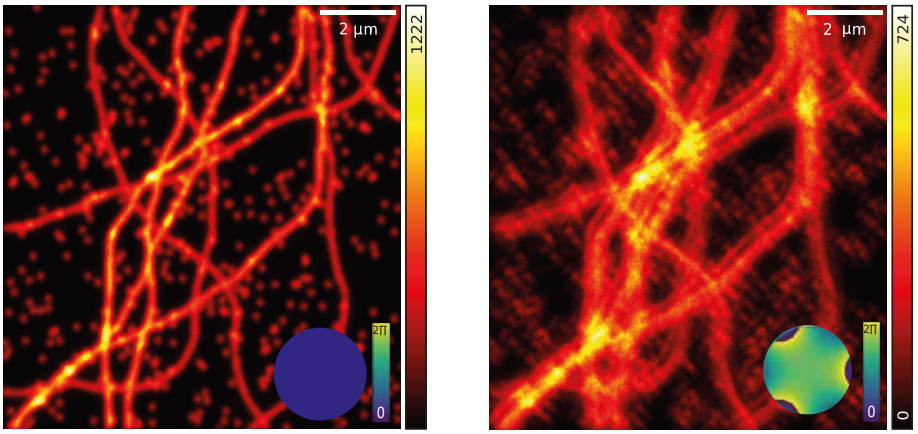

Figure 4. A comparative illustration employing BrightEyes-ISM: on the left, an aberration-free simulation, and on the right, the same phantom convolved with aberrated PSFs altered by applying the desired phase mask. Notably, this comparison highlights the differences in terms of SNR and resolution of the image .

Introducing an optical aberration, such as spherical aberration (Z_0^4 = 1 rad)to modulate the phase mask leads to a modification in the phase propagation of the laser beam during focusing. Consequently, the Point Spread Functions (PSFs) in Image Scanning Microscopy (ISM) are altered compared to the free-aberration case. These changes are reflected in the fingerprint. The fingerprint analysis reveals that the distribution of light extends across all detector elements, resulting

in a decreased Signal-to-Noise Ratio (SNR) and the introduction of artifacts when compared to the aberration-free case fingerprint (see Fig. 5 b). The fingerprint has been demonstrated to be sensitive to optical aberrations in a unique and specific pattern for each aberration.

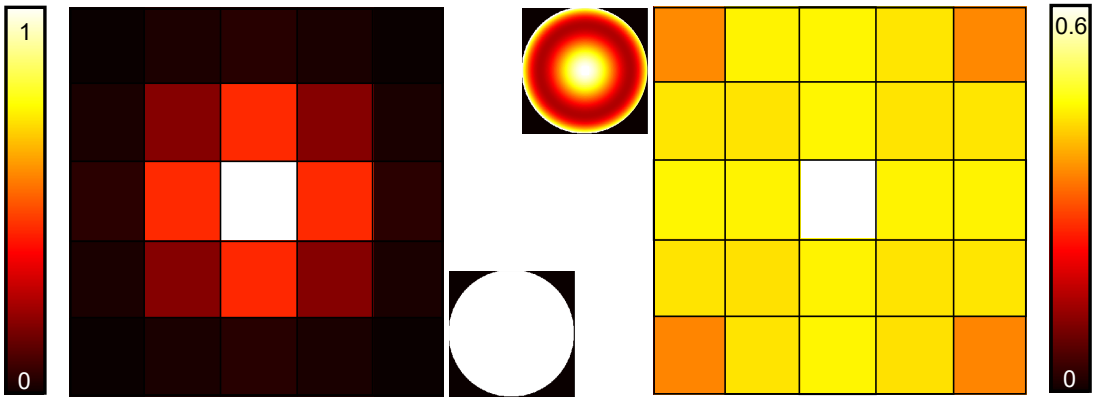

Figure 5. On the left, the fingerprint of a non-aberrated PSF, sharply defined and centered within the active area of the detector array. On the right, the same phantom convoluted with a spherical PSF (using the Zernike polynomial ${Z_0}^4 = 1$ rad), the resulting fingerprint is well-centered yet more dispersed fingerprint across the detector plane. the spherical fingerprint is normalized with respect to the maximum values of the non-aberrated fingerprint.

Furthermore, the phase-correlation method adaptively finds the best estimates of the shift-vectors directly from the scanned images, taking inherently into account non idealities—such optical aberrations without any theoretical assumption. In presence of optical aberrations, the shift-vectors describe a specific and unique pattern, as shown in Fig. 6.

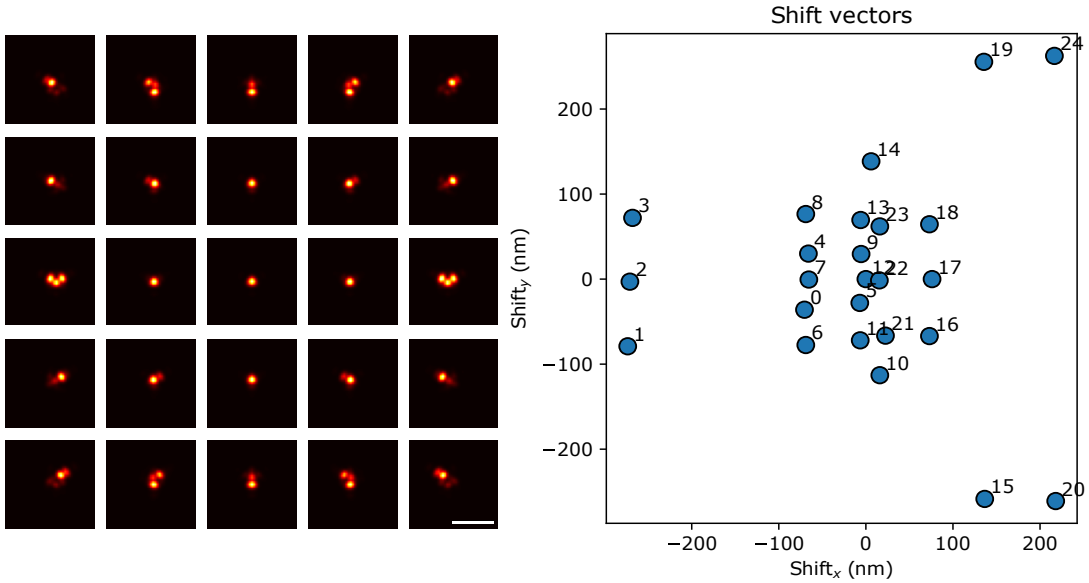

Figure 6. On the left, a set of simulated PSFs, where is applied a phase mask with a vertical trefoil aberration (using the Zernike polynomial ${Z_3}^{-3} = 1$ rad). Notably, the PSFs exhibit variations due to the different perspectives within the matrix structure of the sensor. These PSFs are employed to generate an image from which the shift-vectors are estimated.Scale bar 1 μm.

3. CONCLUSION

In conclusion, our research shows how the ISM dataset obtained by using a detector array naturally encode information about the sample- and system-induced and optical aberration. This ability unlocks new possibilities for adaptive optics (AO) laser

scanning microscopy architectures. Our investigation harnesses the wealth of information provided by the detector array, paving the way for a novel class of systems that seamlessly access and address aberrations. The multi-dimensional dataset, encompassing the fingerprint for direct access to PSFs and shift-vectors for aberration characterization, demonstrates the detector array's remarkable capability in encoding optical aberrations.

To further enhance the estimation of aberration amplitudes, we are currently developing a convolutional neural network (CNN). This CNN will be trained on ISM datasets generated by our simulator, BrightEyes-ISM. The ability to fine-tune parameters with the simulator aims for a generalized applicability of the CNN, extending its utility beyond specific ISM systems.

In essence, our work lays the foundation for a real-time and versatile adaptive optics architecture, enabling precise and efficient aberration estimation directly from experimental images. This breakthrough opens new horizons for deep imaging, marking a significant stride toward advancing the field of optical microscopy.

Acknowledgments

We thank Sabrina Zappone, Andrea Bucci, Giacomo Garré, Sanket Patil, Dr. Mattia Donato, Dr. Eli Slenders, Dr. Marcus Held, and Dr. Eleonora Perego — from Istituto Italiano di Tecnologia — for useful discussions.

REFERENCES

[1] Bertero, M., Boccacci, P., Defrise, M., Mol, C. D., and Pike, E. R., "Super-resolution in confocal scanning microscopy: II. The incoherent case," *Inverse Problems* **5**, 441 (Aug. 1989).

[2] Bertero, M., Brianzi, P., and Pike, E. R., "Super-resolution in confocal scanning microscopy," *Inverse Problems* **3**, 195 (May 1987).

[3] Sheppard, C., "Super-resolution in confocal imaging," *Optik - International Journal for Light and Electron Optics* **80**, 53 (Feb. 1988).

[4] Müller, C. B. and Enderlein, J., "Image scanning microscopy," *Physical Review Letters* **104**, 198101 (May 2010).

[5] Buttafava, M., Villa, F., Castello, M., Tortarolo, G., Conca, E., Sanzaro, M., Piazza, S., Bianchini, P., Diaspro, A., Zappa, F., Vicidomini, G., and Tosi, A., "SPAD-based asynchronous-readout array detectors for image-scanning microscopy," (Feb. 2020). arXiv:2002.11443 [physics].

[6] Slenders, E., Perego, E., Buttafava, M., Tortarolo, G., Conca, E., Zappone, S., Pierzynska-Mach, A., Villa, F., Petrini, E. M., Barberis, A., Tosi, A., and Vicidomini, G., "Cooled SPAD array detector for low light-dose fluorescence laser scanning microscopy," *Biophysical Reports* **1**, None (Dec. 2021).

[7] Castello, M., Tortarolo, G., Buttafava, M., Deguchi, T., Villa, F., Koho, S., Pesce, L., Oneto, M., Pelicci, S., Lanzanó, L., Bianchini, P., Sheppard, C. J. R., Diaspro, A., Tosi, A., and Vicidomini, G., "A robust and versatile platform for image scanning microscopy enabling super-resolution FLIM," *Nature Methods* **16**, 175–178 (Feb. 2019).

[8] Koho, S. V., Slenders, E., Tortarolo, G., Castello, M., Buttafava, M., Villa, F., Tcarenkova, E., Ameloot, M., Bianchini, P., Sheppard, C. J. R., Diaspro, A., Tosi, A., and Vicidomini, G., "Two-photon image-scanning microscopy with SPAD array and blind image reconstruction," *Biomedical Optics Express* **11**, 2905–2924 (June 2020). Publisher: Optica Publishing Group.

[9] Sroda, A., Makowski, A., Tenne, R., Rossman, U., Lubin, G., Oron, D., and Lapkiewicz, R., "SOFISM: Super-resolution optical fluctuation image scanning microscopy," *Optica* **7**, 1308–1316 (Oct. 2020). Publisher: Optica Publishing Group.

[10] Zunino, A., Castello, M., and Vicidomini, G., "Reconstructing the image scanning microscopy dataset: an inverse problem," *Inverse Problems* **39**(6), 064004 (2023). Publisher: IOP Publishing.

[11] Slenders, E., Castello, M., Buttafava, M., Villa, F., Tosi, A., Lanzanò, L., Koho, S. V., and Vicidomini, G., "Confocal-based fluorescence fluctuation spectroscopy with a SPAD array detector," *Light: Science & Applications* **10**, 31 (Feb. 2021). Number: 1 Publisher: Nature Publishing Group.

[12] Tortarolo, G., Zunino, A., Fersini, F., Castello, M., Piazza, S., Sheppard, C. J. R., Bianchini, P., Diaspro, A., Koho, S., and Vicidomini, G., "Focus image scanning microscopy for sharp and gentle super-resolved microscopy," *Nature Communications* **13**, 7723 (Dec. 2022). Number: 1 Publisher: Nature Publishing Group.

[13] Wilson, T., "Resolution and optical sectioning in the confocal microscope," *Journal of Microscopy* **244**(2), 113–121 (2011). _eprint: https://onlinelibrary.wiley.com/doi/pdf/10.1111/j.1365-2818.2011.03549.x.

[14] Conchello, J.-A. and Lichtman, J. W., "Optical sectioning microscopy," *Nature Methods* **2**, 920–931 (Dec. 2005).

[15] Sheppard, C. J. R., "Resolution and super-resolution," *Microscopy Research and Technique* **80**, 590–598 (June 2017).

[16] Booth, M. J., "Wavefront sensorless adaptive optics for large aberrations," *Optics Letters* **32**, 5 (Jan. 2007).

[17] Booth, M. J., Neil, M. A. A., Juškaitis, R., and Wilson, T., "Adaptive aberration correction in a confocal microscope," *Proceedings of the National Academy of Sciences* **99**, 5788–5792 (Apr. 2002).

[18] Linhai, H. and Rao, C., "Wavefront sensorless adaptive optics: a general model-based approach," *Optics Express* **19**, 371 (Jan. 2011).

[19] Kudryashov, A., Samarkin, V., Alexandrov, A., Sheldakova, J., and Zavalova, V., "Shack-Hartmann wavefront sensor - advantages and disadvantages," in [*2010 International Conference on Advanced Optoelectronics and Lasers*], 76–77, IEEE, Sevastopol, Ukraine (Sept. 2010).

[20] Neal, D. R., Copland, J., and Neal, D. A., "Shack-Hartmann wavefront sensor precision and accuracy," in [*Advanced Characterization Techniques for Optical, Semiconductor, and Data Storage Components*], **4779**, 148–160, SPIE (Nov. 2002).

[21] Sheppard, C. J. R., Mehta, S. B., and Heintzmann, R., "Superresolution by image scanning microscopy using pixel reassignment," *Optics Letters* **38**, 2889–2892 (Aug. 2013). Publisher: Optica Publishing Group.

[22] Zunino, A., Slenders, E., Fersini, F., Bucci, A., Donato, M., and Vicidomini, G., "Open-source tools enable accessible and advanced image scanning microscopy data analysis," *Nature Photonics* **17**, 457–458 (June 2023). Number: 6 Publisher: Nature Publishing Group.